Toward a New Type of Multifunctional Metal–Organic Systems Based on Nucleobase Analogues: First Results Derived From The Use of Aliphatic α,ω-Dicarboxylates

ARTICLE *in* CRYSTAL GROWTH & DESIGN · JULY 2012

Impact Factor: 4.89 · DOI: 10.1021/cg300415e

4 AUTHORS, INCLUDING:

Ana B Caballero
University of Barcelona
27 PUBLICATIONS **172** CITATIONS
SEE PROFILE

Luis Lezama
Universidad del País Vasco / Euskal Herriko U…
358 PUBLICATIONS **6,589** CITATIONS
SEE PROFILE

Juan Manuel Salas
University of Granada
265 PUBLICATIONS **3,494** CITATIONS
SEE PROFILE

CRYSTAL GROWTH & DESIGN

Article

pubs.acs.org/crystal

Toward a New Type of Multifunctional Metal–Organic Systems Based on Nucleobase Analogues: First Results Derived From The Use of Aliphatic α,ω-Dicarboxylates

Ana B. Caballero,[†] Antonio Rodríguez-Diéguez,[†] Luis Lezama,[‡] and Juan M. Salas*,[†]

[†]Departamento de Química Inorgánica, Facultad de Ciencias, Universidad de Granada, Avda. Severo Ochoa s/n, E-18071 Granada, Spain

[‡]Departamento de Química Inorgánica, Facultad de Ciencia y Tecnología, Universidad del País Vasco, Apdo. 644, E-48080 Bilbao, Spain

Supporting Information

ABSTRACT: Five new transition metal complexes, containing the purine-mimetic ligands 7-amine-1,2,4-triazolo[1,5-*a*]pyrimidine (7atp) and 4,5-dihydro-5-oxo-1,2,4-triazolo[1,5-*a*]pyrimidine (5HtpO), and also malonate (mal^{2-}) and succinate (suc^{2-}) as secondary ligands are reported. Their formula are $[Mn_2(\mu\text{-}7atp)_2(\mu\text{-}mal)_2(H_2O)_2]$ (**1**), $[Zn_2(\mu\text{-}7atp)_2(\mu\text{-}mal)_2(H_2O)_2]$ (**2**), $[Cu_2(5HtpO)_2(mal)_2(H_2mal)_2(\mu\text{-}H_2O)_2]$ (**3**), $[Cu_2(\mu\text{-}5tpO)_2(\mu\text{-}Hsuc)_2(H_2O)_2]$ (**4**), and $[Cd_2(\mu\text{-}5tpO)_2(\mu_4\text{-}suc)(H_2O)_2]_n$ (**5**). Single-crystal X-ray analysis show that compounds **1**–**4** feature all dinuclear units with different topologies while compound **5** exhibits a 3D-network with small-diameter pores. The variety of coordination modes displayed by both triazolopyrimidine derivatives together with the bridging capability of the aliphatic α,ω-dicarboxylates used lead to compounds with interesting structural features and physical properties. The Cu(II) malonate dimer **3** exhibits weak ferromagnetic interactions (J = +1.5 cm^{-1}) while a weak and a moderately strong antiferromagnetism are displayed, respectively, in the Mn(II) (J = −2.1 cm^{-1}) and Cu(II) succinate dimer **4** (J = −109.7 cm^{-1}). On the other hand, solid-state photoluminescent emission is observed for the Zn(II) compound with a Stokes shift of 73 nm.

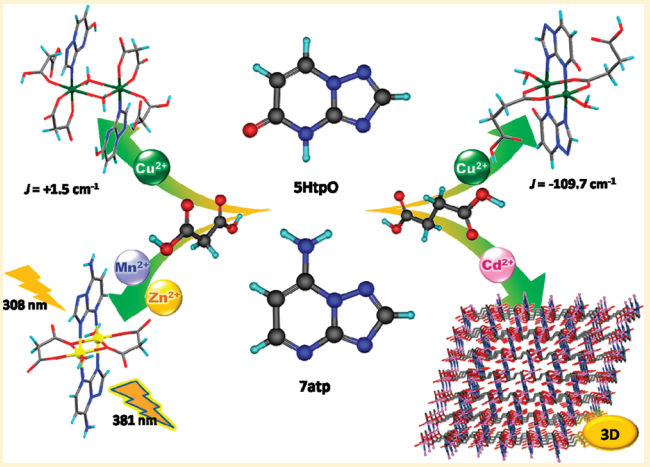

INTRODUCTION

Over the past decades, notable research effort has been invested in the rational design and synthesis of biomimetic systems based on the interaction of biologically relevant molecules with a wide range of organic and inorganic species.[1] The interest in these systems does not only stem from the desire to better understand the complex interactions often present in a great diversity of molecular biorecognition processes[2] but also to afford a powerful tool for the improvement of pharmaceutical agents[3] and the development of artificial receptors used as specific nucleotide sensors or even for the determination of low concentrations of biological and therapeutic agents.[4] In this background, a series of nitrogen heterocycles known as 1,2,4-triazolo[1,5-*a*]pyrimidines may be used as purine analogs (see Scheme 1) to pursue a deeper understanding of interactions between puric nucleobases and metal ions, as well as to obtain new biomimetic systems with interesting properties. The slightly different atomic arrangement in 1,2,4-triazolo[1,5-*a*]pyrimidines might introduce new structural features and different physical and biological properties compared to purine-based systems.[5]

Previous studies have proved a certain versatility of 1,2,4-triazolo[1,5-*a*]pyrimidines as ligands, since they have several nitrogen atoms to bind to metal ions[5,6] (see Scheme 1). Moreover, their coordination ability can be increased by the ring-substitution with functional groups containing donor atoms like nitrogen, sulfur or oxygen, leading to a wider range of coordination modes and structural topologies in their metal complexes.[5−7] Among all already reported coordination modes (more than twelve at present), the most frequent one is the monodentate binding through N3 atom, followed by bidentate through N3 and N4 atoms.[6] In addition, it has been observed than the binding ability of the triazolopyrimidine derivatives is dramatically affected by the metal ion as well as the secondary ligand. It has allowed to establish some

Received: March 28, 2012
Revised: May 8, 2012
Published: May 21, 2012

   dx.doi.org/10.1021/cg300415e | *Cryst. Growth Des.* 2012, 12, 3583–3593

Scheme 1. Ligands 7-Amine-1,2,4-triazolo[1,5-*a*]pyrimidine (7atp) and 4,5-Dihydro-5-oxo-1,2,4-triazolo[1,5-*a*]pyrimidine (5HtpO) and Their Respective Counterpart Nucleobases[a]

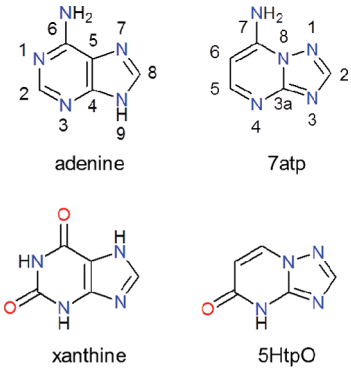

[a]Biochemical and IUPAC ring-numbering system has been employed for purines and 1,2,4-triazolo[1,5-*a*]pyrimidines, respectively.

relationships between the nature of the secondary ligand and the preferred coordination of the triazolopyrimidine, for example, 2,2′-bypirimidine induces a monodentate binding through N3,[8] while monovalent ions like Cu(I) and Ag(I) lead mainly to a N3,N4-bridging fashion.[9a,10] This fact has opened a new research approach to modulate the triazolopyrimidine coordination behavior, thus having recently aroused an increasing interest because of their capability to act as suitable building units for the synthesis of metal−organic multidimensional systems,[9−11] with promising magnetic, luminescent, and to a greater extent, biological properties.[5]

Following the aforementioned research approach, one of our strategies for designing such materials relies on the utilization of multidentate N- or O-donor molecules as secondary ligands which are able to bridge between metal centers to give polymeric structures.[12] In this way, aliphatic *α*,*ω*-dicarboxylates, such as malonate and succinate, are good candidates since both they have proved widely to be very useful tools in crystal engineering and in materials science.[13] The presence of two carboxylate groups in terminal positions and their chain flexibility allow these ligands to adopt several conformations and coordination modes, with more than one of these modes sometimes occurring in the same compound.[14] Moreover, these *α*,*ω*-dicarboxylates show a great capability to establish hydrogen bonding interactions through their carboxylate groups, which is of great interest in biomolecular recognition processes. This phenomenon is strongly pH-dependent, affording thus different protonated forms (desprotonated, monoprotonated, or diprotonated forms) for these ligands.

On this basis, it can be thought that the combined use of oxo- and amine-substituted 1,2,4-triazolo[1,5-*a*]pyrimidine ligands and these aliphatic *α*,*ω*-dicarboxylates might lead to a wide variety of crystal structures ranging from mononuclear species to three-dimensional networks, which may show interesting supramolecular chemistry and physical properties.

In this work, we report the synthesis and the structural characterization -including crystal structure, spectroscopic and thermal analysis- and magnetic and luminescent properties of five mixed ligand metal complexes containing 7-amine-1,2,4-triazolo[1,5-*a*]pyrimidine (7atp) or 4,5-dihydro-5-oxo-1,2,4-triazolo[1,5-*a*]pyrimidine (5HtpO) in presence of malonate or succinate anions: $[Mn_2(\mu\text{-7atp})_2(\mu\text{-mal})_2(H_2O)_2]$ (**1**), $[Zn_2(\mu\text{-7atp})_2(\mu\text{-mal})_2(H_2O)_2]$ (**2**), $[Cu_2(5HtpO)_2(mal)_2(H_2mal)_2(\mu\text{-}H_2O)_2]$ (**3**), $[Cu_2(\mu\text{-5tpO})_2(\mu\text{-Hsuc})_2(H_2O)_2]$ (**4**), and $[Cd_2(\mu\text{-5tpO})_2(\mu_4\text{-suc})(H_2O)_2]_n$ (**5**). Compounds **1**−**4** feature all dinuclear units while compound **5** is a 3D network, with both ligands showing a high variety of binding modes in all them. Apart from a thorough description of their structures, a correlation between these compounds with those reported containing their respective counterpart nucleobases is carried out. Finally, the role that the two types of ligands play in the structure and in the magnetic and luminescent properties of all synthesized compounds will be also discussed. These compounds are the first examples of triazolopyrimidine metal complexes with these dicarboxylate ligands being described.

EXPERIMENTAL SECTION

Mn(II), Zn(II), and Cd(II) carbonates were synthesized by adding the respective metal nitrate salt to an aqueous solution of Na_2CO_3 in a 1:1 molar ratio. The corresponding anhydrous metal carbonate precipitated immediately and was filtered and washed several times with water. Elemental and thermal analyses confirmed anhydrous forms in all cases. The derivative 4,5-dihydro-5-oxo-1,2,4-triazolo[1,5-*a*]pyrimidine (5HtpO) was synthesized as described by Abul-Haj et al.[15] The rest of chemicals were purchased from commercial sources and used without further purification.

Synthesis of $[Mn_2(\mu\text{-7atp})_2(\mu\text{-mal})_2(H_2O)_2]$ (1) and $[Zn_2(\mu\text{-7atp})_2(\mu\text{-mal})_2(H_2O)_2]$ (2). An aqueous suspension containing 0.2 mmol of the respective metal carbonate (0.023 g of $MnCO_3$, 0.025 g $ZnCO_3$), 0.4 mmol of 7atp (0.054 g) and 0.8 mmol of malonic acid (0.083 g) in a total volume of 20 mL was refluxed for 30 min. The suspension turned into a clear yellow solution in both cases. After two weeks standing at room temperature, yellow crystals of complexes **1** and **2** were collected from the respective solutions.

Compound 1. Yield (based on Mn): ∼ 20%. Anal. Calcd. for $C_{16}H_{18}Mn_2N_{10}O_{10}$ (found): C, 30.98 (31.10); H, 2.92 (2.75); N, 22.58 (22.84). Selected IR bands of **1** (cm^{-1}): 1580s ($\nu_{C=O}$), 1627vs, 1668s (ν_{tp}), 3103 m (ν_{N-H}), 3324 m (ν_{O-H}).

Compound 2. Yield (based on Zn) ∼ 50%. Anal. Calcd. for $C_{16}H_{18}N_{10}O_{10}Zn_2$ (found): C, 29.97 (29.79); H, 2.83 (3.39); N, 21.85 (22.56). Selected IR bands of **2** (cm^{-1}): 1584s ($\nu_{C=O}$), 1629vs, 1671s (ν_{tp}), 3081 m (ν_{N-H}), 3307 m (ν_{O-H}).

Preparation of $[Cu_2(5HtpO)_2(mal)_2(H_2mal)_2(\mu\text{-}H_2O)_2]$ (3). An aqueous suspension containing 0.1 mmol of $CuCO_3{\cdot}Cu(OH)_2$ (0.022 g), 0.4 mmol of 5HtpO (0.054 g) and 0.8 mmol of malonic acid (0.083 g) in a volume of 30 mL was refluxed for 1 h, after which the suspension turned into a clear blue solution. The solution was left standing at room temperature and, after a few days, green prismatic crystals of complex **3** were formed in the solution together with colorless crystals of 5HtpO, which were separated each other. Yield (based on Cu): ∼15%. Anal. Calcd. For $C_{22}H_{24}Cu_2N_8O_{20}$ (found): C, 31.18 (31.60); H, 2.85 (2.99); N, 13.22 (13.03). Selected IR bands of **3** (cm^{-1}): 1578s ($\nu_{C=O}$, malonate), 1637 m, 1716vs (ν_{tp} + ν_{pym} + $\nu_{C=O}$, 5HtpO), 3417 m (ν_{O-H}).

Preparation of $[Cu_2(\mu\text{-5tpO})_2(\mu\text{-Hsuc})_2(H_2O)_2]$ (4) and $[Cd_2(\mu\text{-5tpO})_2(\mu_4\text{-suc})(H_2O)_2]_n$ (5). An aqueous suspension containing the respective metal carbonate (0.1 mmol $CuCO_3{\cdot}Cu(OH)_2$, 0.022 g; 0.2 mmol $CdCO_3$, 0.034 g), 0.2 mmol of 5HtpO (0.027 g) and 0.6 mmol of succinic acid (0.071 g) in a volume of 20 mL was refluxed for 30 min. The suspension of Cd turned into a colorless solution but in case of Cu, copper succinate was formed and was filtered off leaving a clear blue solution. After 2−3 weeks at room temperature, blue crystals of **4** and colorless crystals of **5** were collected from the respective solutions, in both cases together with colorless crystals of 5HtpO.

Compound 4. Yield (based on Cu): ∼10%. Anal. Calcd for $C_{18}H_{20}Cu_2N_8O_{12}$ (found): C, 32.39 (32.20); H, 3.02 (3.29); N, 16.79 (16.81). Selected IR bands of **4** (cm^{-1}): 1439s, 1642s ($\nu_{C=O}$, succinate), 1509vs, 1562s, 1736s (ν_{tp} + ν_{pym} + $\nu_{C=O}$, 5tpO$^-$), 3265 m (ν_{O-H}).

dx.doi.org/10.1021/cg300415e | *Cryst. Growth Des.* 2012, 12, 3583−3593

Table 1. Crystal Data and Structure Refinement of 1−5

	1	2	3	4	5
empirical formula	$C_{16}H_{18}Mn_2N_{10}O_{10}$	$C_{16}H_{18}N_{10}O_{10}Zn_2$	$C_{22}H_{24}Cu_2N_8O_{20}$	$C_{18}H_{20}Cu_2N_8O_{12}$	$C_7H_7CdN_4O_4$
M (g mol^{-1})	620.28	641.14	847.57	667.50	323.57
crystal size (mm)	0.27 × 0.15 × 0.10	0.19 × 0.10 × 0.03	0.21 × 0.17 × 0.11	0.24 × 0.18 × 0.12	0.18 × 0.13 × 0.10
crystal appearance	prism, pale-yellow	prism, yellow	prism, green	prism, blue	prism, colorless
2θ range (deg)	4.80−50.00	4.82−50.00	4.18−50.00	4.80−49.76	5.02−50.00
h, k, l range	±11, ±8, ±18	±11, ±8, ±17	±10, ±10, ±11	±10, −16−18, −7−10	±14, ±13, ±16
temp (K)	100	100	100	100	100
crystal system	monoclinic	monoclinic	triclinic	monoclinic	monoclinic
space group	$P2_1/n$	$P2_1/n$	$P\bar{1}$	$P2_1/c$	$C2/c$
a (Å)	9.8898(7)	9.852(5)	9.049(1)	8.602(5)	11.9080(9)
b (Å)	7.4858(6)	7.378(5)	9.243(1)	15.692(5)	11.4930(11)
c (Å)	15.2851(11)	15.129(5)	9.967(1)	8.868(5)	14.2810(11)
α (deg)	90.00	90.00	93.230(2)	90.000	90.00
β (deg)	92.6490(10)	93.037(5)	98.632(2)	99.769(5)	106.227(8)
γ (deg)	90.00	90.00	115.281(1)	90.000	90.00
V (Å^3)	1130.39(15)	1098.2(10)	738.5(2)	1179.7(10)	1876.6(3)
Z	2	2	1	2	8
D_{calcd} (g cm^{-3})	1.822	1.939	1.906	1.879	2.290
$F(000)$	628	648	430	676	1256
μ (mm^{-1})	1.195	2.265	1.548	1.886	2.333
max/min transmission	0.868/1.000	0.860/1.000	0.838/1.000	0.783/1.000	0.920/1.000
reflections collected	10668	10338	7198	6170	4945
indep. reflections (R_{int})	1990 (0.0260)	1932 (0.0492)	2585 (0.0304)	2040 (0.1183)	1653 (0.0217)
obs. reflect [$I > 2\sigma(I)$]	1853	1581	2214	1195	1484
parameters refined	180	188	255	193	153
max./min. $\Delta\rho^a$ (/e Å^{-3})	0.353/-0.183	0.489/-0.352	0.513/-0.325	0.983/-0.560	0.777/-0.561
R_1/R_2 [$I > 2\sigma(I)$]^b	0.0277/0.0694	0.0435/0.0881	0.0418/0.1012	0.0654/0.1310	0.0234/0.0585
R_1/R_2 (all reflns)^b	0.0303/0.0709	0.0581/0.0936	0.0499/0.1088	0.1203/0.1598	0.0265/0.0604
goodness-of-fit on F^2 ^{c}	1.039	1.074	1.043	0.971	1.064
weight. scheme w; a/b^d	0.0329/0.8435	0.0321/2.5720	0.0544/0.4349	0.0000/0.0000	0.0359/0.0000

^{a}Largest difference peak and hole. $^b R_1 = [\Sigma(||F_o| - |F_c||)/\Sigma|F_o|]$; $R_2 = [\Sigma\{w(F_o^2 - F_c^2)^2\}/\Sigma[w(F_o^2)^2]]^{1/2}$. ^{c}Goodness-of-fit = $[\Sigma[w(F_o^2 - F_c^2)^2]/(n - p)]^{1/2}$. $^d w = 1/[\sigma^2(F_o^2) + (\alpha P)^2 + bP]$ where $P = (\max(F_o^2 \text{ or } 0) + 2F_c^2)/3$.

Compound **5**. Yield (based on Cd): ∼60%. Anal. Calcd for $C_7H_7CdN_4O_4$ (found): C, 25.98 (26.50); H, 2.18 (2.19); N, 17.31 (17.33). Selected IR bands of **5** (cm^{-1}): 1426s, 1459vs, 1631vs ($\nu_{C=O}$, succinate), 1552vs ($\nu_{tp} + \nu_{pym} + \nu_{C=O}$, 5tpO$^-$), 3392 m ($\nu_{O-H}$).

X-ray Crystal Structure Analysis. *Data Collection.* Bruker Smart Apex CCD diffractometer with Mo Kα radiation (λ = 0.71073 Å), graphite monochromator, ω- and ϕ-scan; data collection with Apex2,[16] cell refinement and data reduction with SAINT,[16] and experimental absorption correction with SADABS.[17]

Structure Analysis and Refinement. The structures of **1**−**5** were solved by direct methods using SIR97;[18] refinement was done by full-matrix least-squares on F^2 using the SHELXL-97 program suite.[19] All non-hydrogen positions were refined with anisotropic displacement parameters. Hydrogen atoms were positioned geometrically and refined using riding models with $U_{iso}(H) = 1.2U_{eq}(CH, CH_2)$ and $U_{iso}(H) = 1.5U_{eq}(CH_3)$.

Crystal data and details on the structure refinement are given in Table 1. The structural data have been deposited with the Cambridge Crystallographic Data Center: CCDC-835133 (**1**), −835134 (**2**), −835135 (**3**), −835136 (**4**), and −835137 (**5**).

Physical Measurements. Elemental analyses were performed on a Fisons-Carlo Erba analyzer model EA 1108. The IR spectra on powdered samples were recorded with a ThermoNicolet IR200FTIR by using KBr pellets. Thermal behavior was studied under an air flow in Shimadzu TGA-50 and Shimadzu DSC-50 equipment, at heating rates of 20 and 10 °C min^{-1}, respectively. Reflectance diffuse spectra were measured on a VARIAN model CARY-5E spectrophotometer. Magnetization and variable temperature (1.9−300 K) magnetic susceptibility measurements on polycrystalline samples were carried out on a Quantum Design SQUID MPMS XL-5 device operating at 0.1 T for the compounds **1**, **3**, and **4**. Magnetization measurements at 2 K were obtained in a Vibrating Sample Magnetometer (CFMS, Cryogenic Ltd.). The experimental susceptibilities were corrected for the diamagnetism of the constituent atoms by using Pascal tables. X-Band EPR measurements were registered on a Bruker ELEXSYS 500 spectrometer with a maximum available microwave power of 200 mW and equipped with a superhigh-Q resonator ER-4123-SHQ. For Q-band studies, EPR spectra were recorded on a Bruker EMX system equipped with an ER-510-QT resonator and a ER-4112-HV liquid helium cryostat. The magnetic field was calibrated by a NMR probe and the frequency inside the cavity was determined with a Hewlett-Packard 5352B microwave frequency counter.

Luminescence Measurements. A Varian Cary-Eclipse Fluorescence Spectrofluorimeter solid sample holder accessory was used to obtain the fluorescence spectra at room temperature. The spectrofluorimeter was equipped with a xenon discharge lamp (peak power equivalent to 75 kW), Czerny-Turner monochromators, R-928 photomultiplier tube which is red sensitive (even 900 nm) with manual or automatic voltage controlled using the Cary Eclipse software for Windows 95/98/NT system. The photomultiplier detector voltage was 700 V and the instrument excitation and emission slits were set at 5 and 5 nm, respectively.

RESULTS AND DISCUSSION

Spectroscopic (IR and Solid UV−vis) and Thermal Characterization. The 1500−1700 cm^{-1} region of the infrared spectra of the free triazolopyrimidine ligands displays three main characteristic bands for 7atp (1680, 1656, and 1573 cm^{-1})[20] and an intense band in the C=O region at 1685 cm^{-1},

dx.doi.org/10.1021/cg300415e | Cryst. Growth Des. 2012, 12, 3583−3593

with two shoulders at 1713 and 1738 cm^{-1} for 5HtpO,[21] which are slightly affected by the metal coordination in compounds **1**, **2**, and **3**. The spectra of **4** and **5**, with the 5HtpO ligand in its anionic form, display both the expected shift of this band to lower wavenumber, showing a single narrow band at 1736 cm^{-1} and 1552 cm^{-1}, respectively; the extra shift in the latter being perhaps Because of the involvement of O5 in coordination.[22] The presence of the malonate and succinate anions is indicated by the typical stretching vibrations of carboxylic C═O bonds, through intense bands around 1580 cm^{-1} for malonate and around 1450 and 1635 cm^{-1} for succinate.

The diffuse reflectance spectra for Cu(II) compounds present an only broad and asymmetric band with a maximum at 12484 cm^{-1} for **3** and 15106 cm^{-1} for **4**. These relatively low values for Δ_o indicate a predominance of oxygen atoms in the metal coordination sphere.

All compounds are thermally stable until 180−200 °C. Thermal decomposition begins with the loss of coordination water molecules, being this process overlapped with the decarboxylation of malonate or succinate ligand present in the compounds. Both processes take place together in a single-step weight loss in the temperature range 180−250 °C (see TG and DSC of **4**, Supporting Information Figure S1). In DSC diagrams, these processes appear also together as one intense and well-defined endothermic effect in the temperature interval between 200 and 230 °C, except for **3**, where this endothermic effect is centered at 167.8 °C. The pyrolysis of the organic moiety occurs in one or two steps and begins around 300 °C for all compounds, leaving the corresponding metal oxide (CuO, ZnO, and CdO) or dioxide (MnO_2) as inorganic residue.

Crystal Structures. Compounds **1** and **2** with the 7-amine-1,2,4-triazolo[1,5-*a*]pyrimidine (7atp) ligand are isostructural. Both compounds feature a centrosymmetric dinuclear molecular unit $[M_2(\mu\text{-7atp})_2(\mu\text{-mal})_2(H_2O)_2]$ (Figure 1), in which

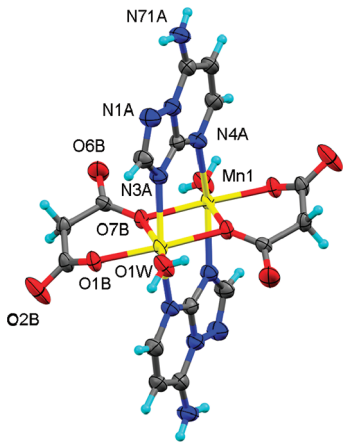

Figure 1. Molecular dinuclear unit of metal complex **1**, isostructural with **2** (50% probability ellipsoids). Selected bond distances and angles are given in Supporting Information Table S1.

the metal ion (M = Mn^{2+}, Zn^{2+}) is coordinated by the triazole−N3 and the pyrimidine-N4 atoms, three oxygen atoms from the malonate ligands and one water molecule in a distorted octahedral geometry. M−N3 and M−N4 bond distances are in the same order than those for other nondicarboxylate-containing complexes, and are both longer for the manganese(II) complex (2.282(2) and 2.298(2) Å, respectively) than for the zinc(II) compound (2.171(5) and 2.184(5) Å, respectively).

The metal centers within the dinuclear entities are bridged by two malonate anions and two 7atp molecules to give a "paddle-wheel" motif, with M···M distances 3.1988(6) and 3.123(2) Å for **1** and **2**, respectively. In compounds **1** and **2**, 7atp bridging ligands present a head−tail nearly coplanar arrangement and display a μ−κN3:κN4 coordination mode, which has been shown in the two previously reported compounds with this ligand, $[Ag_2(\mu\text{-7atp})_2](ClO_4)_2$[10] and $[Cu_2(\mu\text{-7atp})_4(H_2O)_2](ClO_4)_4{\cdot}3H_2O$.[23] However, unlike both these complexes, 7atp bicyclic rings are not coplanar or contained in parallel planes in **1** and **2**, but forming a dihedral angle of 1.82° between their mean planes. On the other hand, the malonate anion shows an unusual tridentate μ-κ^2O1,O7:κO7 coordination mode where O7B links the two metal atoms and O1B is bonded only to one of these metal centers, thus forming a six-membered chelate ring. The presence of multiple hydrogen donors and acceptors in the molecule generates a complex three-dimensional hydrogen-bond network, in which all 7atp amine groups, water molecules and carboxylic oxygen atoms are taking part with D···A distances ranging from 2.637 Å to 3.052 Å.

When the oxo-derivative 5HtpO was made to react in presence of malonate anion and several first-row transition metal ions (from Mn(II) to Zn(II)), only the copper(II) compound **3** was isolated as single-crystal. Its structure consists of centrosymmetric dinuclear units which differ significantly from dimers **1** and **2**, since metal ions are bridged this time through two water molecules. Moreover, in compound **3** just one triazolopyrimidine ligand coordinates each Cu(II) and in a N3-monodentate fashion while three oxygen atoms from two malonate ligands complete a distorted octahedral coordination sphere. The most outstanding feature is that two different forms of the secondary ligand occur in the same compound, the neutral form (H_2mal) and the fully deprotonated anion (mal^{2-}). The neutral form coordinates monodentately by one carboxylic oxygen (Cu−O2C = 2.366(3) Å) while the malonate anion displays a bidentate κ2O2B,O6B coordination mode with shorter metal binding distances (Cu−O2B = 1.920(3) Å; Cu−O6B = 1.936(2) Å). Other coordination bond distances for this compound are listed in Supporting Information Table S1. The intermetallic distance of the dioxo-type bridge is 3.701(1) Å, and it is not symmetric (two different Cu−Ow distances: 2.012(3) and 2.681(3) Å). Coordinated malonic acid molecules link neighboring dinuclear entities by hydrogen bonds generating supramolecular chains, as shown in Figure 2. These supramolecular chains are assembled by strong π-stacking interactions between 5HtpO triazolic rings with a rather short centroid-centroid contact (3.482 Å) and with a good overlap of the aromatic planes, building then a 2D-network.

Different structural topologies are generated by using succinate instead of malonate as secondary ligand. The copper(II) complex **4** consists of molecular dinuclear entities which are centrosymmetric. Unlike dimer **3**, in the complex **4** each Cu(II) ion displays an almost perfect square pyramidal coordination geometry with a trigonality index τ_5 = 0.09.[24] Moreover, the 5HtpO ligands occur in anionic form of 5HtpO ($5tpO^-$) and are both coplanarly arranged, acting as bridging ligands through N3 and N4 with metal binding distances of 2.006(6) and 2.012(6) Å, respectively. Two succinate anions in its monoprotonated form ($Hsuc^-$) share the bridging role of $5tpO^-$ by binding through the two oxygen atoms of one

dx.doi.org/10.1021/cg300415e | *Cryst. Growth Des.* 2012, 12, 3583−3593

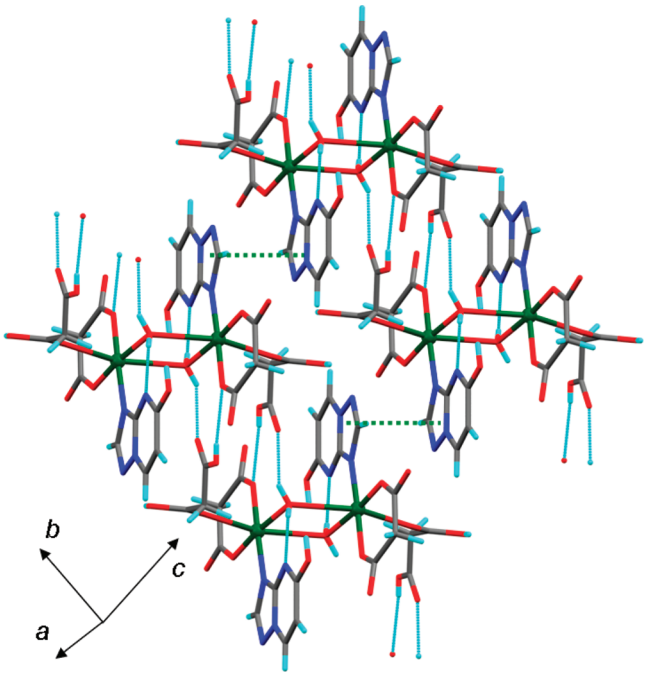

Figure 2. Section of the packing in compound **3**, showing the supramolecular chains built by hydrogen bonds and their π-stacking assembly.

carboxylate group (Figure 3). Selected distances for the coordination polyhedron of **4** are given in Supporting Information Table S1. Their second carboxylic group keeps protonated and interacting by strong hydrogen bonds (O8B···N1A = 2.806 Å) with the triazolic N1 atom of neighboring dinuclear entities, building a supramolecular chain substructure as shown in the Figure 3. Water molecules and 5tpO$^-$ oxygen atom (O51) also take part in the formation of hydrogen bonds giving rise to a three-dimensional network.

In this dinuclear compound, a quite short Cu–Cu bond, 2.776(1) Å, is generated by the bridging action of the 5HtpO ligands and succinate together. To the best of our knowledge, this distance is the shortest observed in a metal complex with a triazolopyrimidine derivative and it suggests the existence of a significative interaction between both Cu(II) ions, which logically has relevant consequences in the magnetic properties of the compound (shown in EPR and Magnetic Properties section).

The crystal structure of the compound $[Cd_2(\mu\text{-}5tpO)_2(\mu_4\text{-}suc)(H_2O)_2]_n$ (**5**) is rather different from the above-described complexes **1**–**4**. It consists of a three-dimensional covalent network, in which Cd(II) ions show a coordination index of 7 and an unusual coordination geometry intermediate between capped trigonal prismatic and capped octahedral. The coordination sphere is formed by two nitrogen atoms (N3A, N4A) and one oxygen atom (O51A) belonging to two monodeprotonated 5HtpO derivatives, three oxygen atoms from two succinate anions and one oxygen atom from a water molecule. It should be noted that three different intermetallic bridges coexist in the structure, as observed in Figure 4. First,

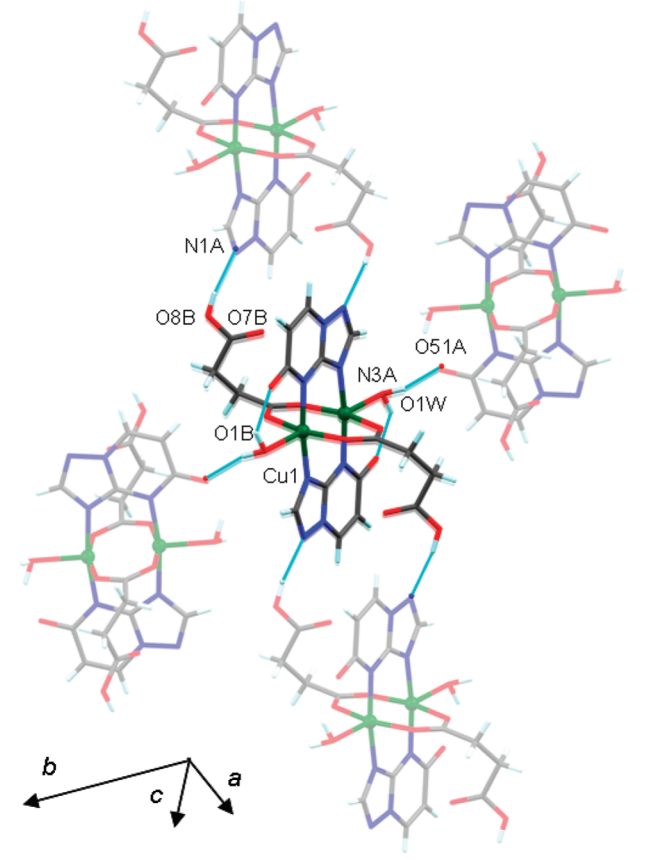

Figure 3. Molecular dinuclear unit of compound **4**. Formation of hydrogen bonds to generate the 3D supramolecular network.

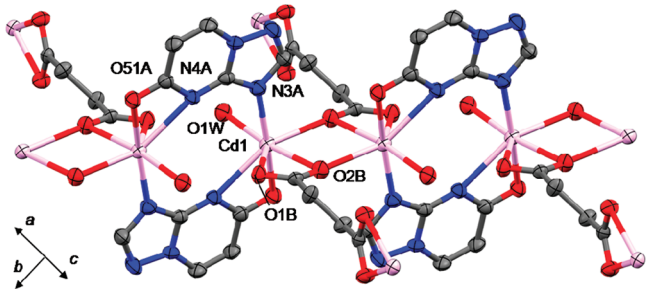

Figure 4. View of the metal environments in compound **5** where the three types of intermetallic bridges are showed (50% probability ellipsoids). Hydrogen atoms are omitted for clarity.

two 5tpO$^-$ moieties are bridging two metal centers in a μ-κ^2N4,O5:κN3 fashion (Cd···Cd 4.6412(4) Å). Despite the possible involvement of the exocyclic oxygen atom in coordination was predicted previously for 5HtpO from theoretical calculations,[15] compound **5** is the first example in the literature where this derivative displays such coordination binding, probably favored by the bigger size of the metal ion compared with other second-row transition metal ions like Pt(II) and Pd(II) and those of the first-row. On the other hand, succinate anions connect metal ions in two different ways: (i) bridging four metal ions through its carbonated skeleton in a μ_4-κ^2O1B,O2B:κO2B:κ^2O1B,O2B:κO2B coordination mode, which gives rise to the longest Cd···Cd distance in the structure, 9.3409(8) Å; (ii) each carboxylate group is bridging two Cd(II) ions respectively through one oxygen atom while the another oxygen is also coordinated to one of these metal centers, resulting in a κ^2O1B,O2B:κO1B binding mode. The intermetallic distance generated by this bridging mode is 3.9927(4) Å, the shortest one of the structure. The O1B–

dx.doi.org/10.1021/cg300415e | *Cryst. Growth Des.* 2012, 12, 3583–3593

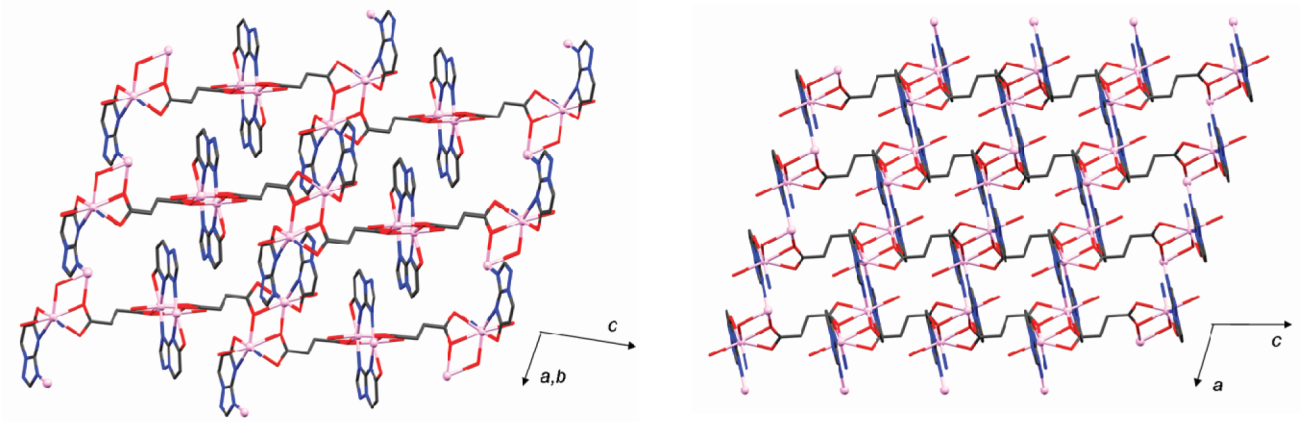

Figure 5. Perspective views of the 3D network of compound **5**, showing the pores formed along two different directions. Hydrogen atoms are omitted for clarity.

Cd1−O2B chelate angle is rather small, only 58.05(7)°. That chelating interaction together with that formed by N4,O5-chelating binding of 5HtpO ligands (N4A−Cd1−O51A = 54.96(8)°) are both mainly responsible of the significant distortion suffered in coordination polyhedra. Selected bond distances of coordination polyhedra in this complex are given in Supporting Information Table S1.

As a consequence of this coordination mode, small-diameter pores are generated in the polymeric network of **5** as observed in Figure 5. In the view on the left, it can be clearly observed that the three-dimensional network is made up of dinuclear substructures which resemble dimers **1**, **2**, and **4** reported herein. In these subentities, 5tpO$^-$ anions keep coplanarly arranged in a head−tail fashion. However, the intermetallic distance is much longer in these dinuclear substructures probably because of the bigger atomic size of Cd(II) ions if compared with the first-row transition metal ions. This fact may prevent succinate anions from forming a carboxylate-bridge between both metal centers.

From all results described above we can conclude that the oxo-derivative 5HtpO shows a clear preference for interacting through at least N3 and N4 atoms simultaneously. This fact is in good agreement with reported literature on metal complexes with this derivative.[9] Only in compound **3**, this ligand binds monodentately by N3.

Although the two triazolopyrimidine derivatives which are studied in the present work show three different coordination modes, N3-monodentate, N3,N4-bridging and N3,N4,O5-bridging, the structural versatility displayed in compounds **1**-**5** seems to be mainly due to the also different binding behavior of the *α*,*ω*-dicarboxylate, as both together display as much as four different coordination fashions. Thus, these preliminary results prove that these two difunctionalized ligands may be quite useful for the synthesis of further multidimensional compounds based on biomimetic ligands such as 1,2,4-triazolo[1,5-*a*]pyrimidines, aimed to enhance the physical properties of the already existing compounds based on these heterocycles.

EPR and Magnetic Properties. X and Q-band EPR measurements for compounds **1**, **3** and **4** were carried out on powdered samples at several temperatures in the range 4−300 K. In all cases, the spin Hamiltonian parameters were estimated by comparison of the experimental spectra with those obtained by a computer simulation program working at the second order of the perturbation theory. The room temperature EPR spectrum of **1** (Figure S2, Supporting Information) is characteristic of a d^5 metal ion as Mn(II), with g value around 2 and a *D* value lower than 0.1 cm^{-1}. The spectrum is poorly resolved by the effect of relatively large line widths caused by the dipolar interactions between the metal centers (Mn···Mn distance: 3.199 Å). When lowering temperature the resolution of the spectra is improved, but the intensity of the signal decreases below 30 K suggesting the presence of antiferromagnetic exchange interactions.

The EPR spectrum obtained for a powdered sample of complex **3** (Figure S3, Supporting Information) exhibits a rhombic symmetry (almost axial) for the *g* tensor, with the following main values: g_1 = 2.336, g_2 = 2.085, and g_3 = 2.077. These values are typical of Cu(II) ions in axially elongated environments, in good agreement with the structural characteristics of the centrosymmetric dinuclear units of this compound. Moreover, the absence of "half-field" transitions or hyperfine lines indicates the presence of some type of extended magnetic exchange, probably via hydrogen bonding. In any case, the intra- and interdimeric exchange must necessarily be weak considering that the spectra remain unchanged when cooling down to 4.2 K.

The EPR spectrum of compound **4** measured in the Q-band (shown in Figure 6) is characteristic of a triplet *S* = 1 state with appreciable zero field splitting, which probably arises from the

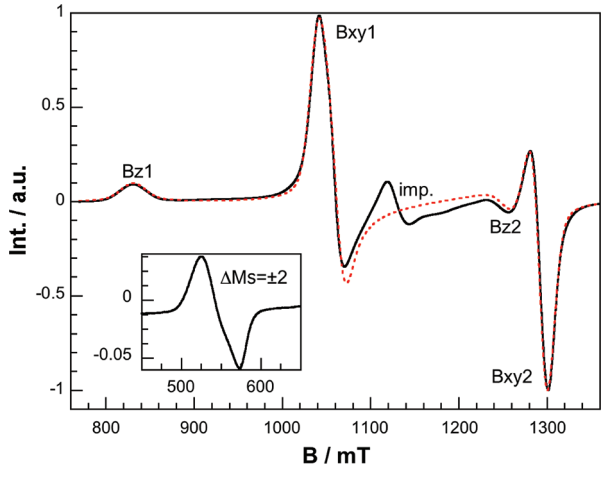

Figure 6. Room temperature Q-band EPR spectrum of compound **4**. Dashed line is the best fit; see text for the fitting parameters.

dx.doi.org/10.1021/cg300415e | *Cryst. Growth Des.* 2012, 12, 3583−3593

combined effects of the anisotropic exchange coupling and from the classical dipole−dipole interaction. It could be interpreted on the basis of the following spin Hamiltonian:

$$H_{ss} = \beta B\mathbf{gS} + D(\mathbf{S}_z^2 - 2/3) + E(\mathbf{S}_x^2 - \mathbf{S}_y^2) \quad (1)$$

where D and E are the axial and rhombic zero field splitting parameters, respectively. Simulations of the powder pattern allowed to determine the parameters: $g_1 = 2.325$, $g_2 = 2.073$, $g_3 = 2.060$, $|D| = 0.236$ cm^{-1}, and $|E| = 0.005$ cm^{-1}. These values were used to simulate the powder EPR spectrum in order to produce the dashed line in Figure 6. The fit of all signals was satisfactory with the exception of a central line (ca. 1130 mT), which can be assigned to a small $S = 1/2$ signal of a mononuclear Cu(II) impurity also observed in the magnetic susceptibility measurements.

The g values are typical of Cu(II) ions in square pyramidal geometries with the unpaired electron on the $d_{x^2-y^2}$ orbital. The calculated D parameter is intermediate between those found for dimers with only carboxylate bridges (0.3−0.4 cm^{-1}) and those reported for analogous compounds with nitrogen donor atoms in the bridges (0.1−0.2 cm^{-1}). A similar behavior has been previously observed in related systems.[25]

The knowledge of the sign of the D parameter is not available from powder low frequency EPR or magnetic susceptibility measurements. However, by means of single-crystal EPR measurements at high frequencies (435 GHz), Ozarowski[26] has demonstrated that D is negative in all binuclear copper carboxylates exhibiting the "paddlewheel" and related structures. Therefore, one can extract the anisotropic exchange contribution to the zero-field splitting, D_{ex}, from the experimental D parameter simply subtracting the dipole−dipole part: $D = D_{ex} + D_{dip}$. Moreover, in compound **4** the Cu−Cu and the g_z direction must be very close to each other, thus the dipole−dipole contribution can be calculated with the following formula based on a point dipole model[27]

$$D_{dip} = -[2g_z^2 + (g_x^2 + g_y^2)/2]\beta/2(r_{Cu-Cu})^3 \quad (2)$$

which results in −0.165 cm^{-1} for compound **4** ($r_{Cu-Cu} = 2.776$ Å), so that the calculated value of D_{ex} is −0.071 cm^{-1}. From this value, one can deduced the triplet-singlet separation in dimeric excited states where one cupric ion is in its electronic ground state ($d_{x^2-y^2}$) while another one is in an excited state d_{xy}[28]

$$D_{ex} = J(x^2 - y^2, xy)(g_z - 2.0023)^2/32 \quad (3)$$

Therefore, the $J(x^2 - y^2, xy)$ is approximately −20 cm^{-1}, which corresponds to a weak ferromagnetic exchange in the corresponding excited state of the dimer, in good agreement with the orthogonal arrangement of the $d_{x^2-y^2}$ and d_{xy} magnetic orbitals. It is noteworthy that the relationship between this splitting within the excited state of the dimer and the ground state exchange integral (J) is still unknown.

Variable-temperature magnetic susceptibility measurements were carried out on powdered samples of the complexes **1**, **3** and **4** in the 1.9−300 K temperature range. The plots of magnetic molar susceptibility (χ_m) and $\chi_m T$ product ($\chi_m T = (\mu_{eff})^2/8$) versus temperature are shown in Figure 7. The magnetic susceptibility of compound **1** shows a maximum around 17 K and the high temperature data (100−300 K) can be fitted to the Curie−Weiss law with $C_m = 8.64$ cm^{3}K/mol and θ =-18.8 K. Upon cooling, the magnetic effective moment shows a continuous decrease from 11.4 μ_B at room temperature

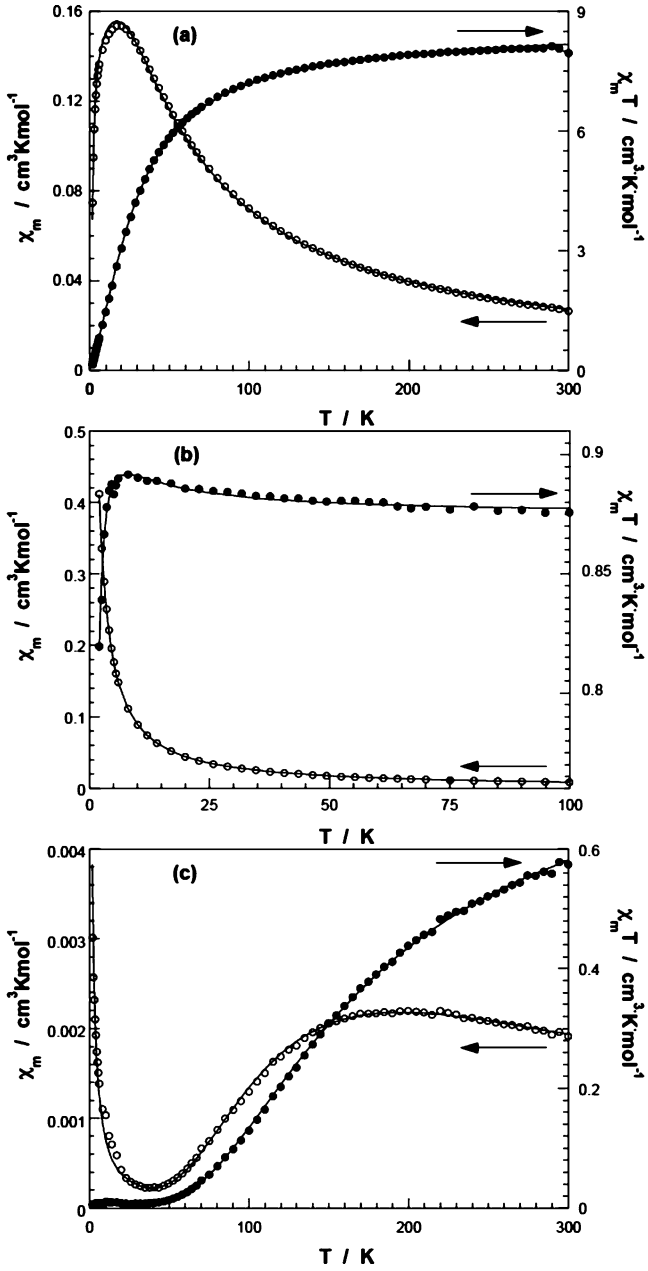

Figure 7. Plots of χ_m and $\chi_m T$ vs T for complexes **1** (a), **3** (b), and **4** (c). The solid lines correspond to the best theoretical fits (see text).

(close to the calculated spin-only value of 11.8 μ_B for two independent high-spin d^5 ions) to 1.5 μ_B at 2 K. This behavior is indicative of the presence of antiferromagnetic interactions between the Mn(II) ions. We have analyzed the experimental magnetic data by fitting to eq 1 derived from the isotropic Heisenberg exchange Hamiltonian $H = -2JS_1S_2$ and obtained by substituting the values for the Mn^{2+} ion into the van Vleck equation[29]

$$\chi_m = \frac{Ng^2\beta^2}{kT}\frac{55 + 30x^{10} + 14x^{18} + 5x^{24} + x^{28}}{11 + 9x^{10} + 7x^{18} + 5x^{24} + 3x^{28} + x^{30}} \quad (4)$$

where $x = \exp(-J/kT)$, J is the exchange integral and g is the Lande's g factor; N, β, and k are the Avogadro's number, the Bohr magneton, and Boltzmann's constant, respectively. The best-fit parameters obtained by minimizing the reliability R

dx.doi.org/10.1021/cg300415e | Cryst. Growth Des. 2012, 12, 3583−3593

factor, $R = \Sigma[(\chi_m T)_{exp} - (\chi_m T)_{cal}]^2/\Sigma[(\chi_m T)_{exp}]^2$, are $g = 1.99$, $J = -2.1$ cm^{-1} and $R = 3.5 \times 10^{-5}$.

It is well-known that nonlinear NCN bridges cause antiferromagnetic coupling[30] while μ-oxo bridges are able to transmit both ferromagnetic and antiferromagnetic interactions depending on the M−O−M angle and the orientation of the metal-centerd magnetic orbitals.[31] As for Mn(II) ions μ-oxo bridges transmit mostly antiferromagnetic interactions, then the two bridging ligands in compound **1** would add their effects, being this phenomenon known as orbital complementarity.[32,33] Although no other Mn(II) dimer with similar connection between both centers to that in compound **1** has been found in the literature, the aforementioned phenomenon could justify why the magnetic coupling of this dimer is higher than those for other Mn(II) dimers with only two N−C−C−N bridges and shorter intermetallic distance.[34]

At room temperature the $\chi_m T$ value of compound **3** is 0.875 cm^{3}K/mol which is close to the expected value for two uncoupled copper(II) ions with $g = 2.166$ (see EPR results). The magnetic effective moment increases slightly when temperature is lowered and $\chi_m T$ reaches a maximum of 0.892 cm^3 K/mol at about 8 K. Below this temperature $\chi_m T$ decreases to a value of 0.819 cm^3 K/mol at 2 K. This behavior indicates predominant ferromagnetic coupling between copper(II) ions bridged by water molecules. The low temperature decrease of the magnetic effective moment can be ascribed to the presence of interdimeric antiferromagnetic exchange or the zero-field splitting of the $S = 1$ ground state. To determine the exchange parameter we have used the Bleaney−Bowers expression for an isotropically coupled pair of $S = 1/2$ ions,[35] including a Curie−Weiss correction

$$\chi_m = \frac{Ng^2\beta^2}{k(T - \theta)(3 + 3\exp(-J/kT)} \quad (5)$$

where the singlet−triplet energy gap ($2J$) is defined by the Hamiltonian $H = -2JS_1 \cdot S_2$ ($S_1 = S_2 = 1/2$). The magnetic parameters obtained from the best fit are $g = 2.16$, $J = +1.5$ cm^{-1}, and $\theta = -0.74$ K, with $R = 6.3 \times 10^{-6}$. As shown in Figure 7b, calculated curves reproduce satisfactorily the experimental data in the whole investigated temperature range. The small, but positive, value of J for this compound has been also manifested by the curve of the reduced magnetization ($M/N\beta$) versus applied field H, measured at 2 K, compared with the theoretical Brillouin law for two isolated copper(II) ions. The experimental curve lies slightly above the theoretical Brillouin curve (Figure S4, Supporting Information), indicating a very small ferromagnetic coupling. This behavior is related to the asymmetric coordination of the water molecules to the copper(II) ions, with short and long Cu−N bond lengths in the bridges equal to 2.012(3) and 2.681(3) Å, respectively. Moreover, the water molecules bridge the apical positions of one copper atom and the equatorial plane of the adjacent copper atom. Thus, the two metal-centered magnetic orbitals (mainly $d_{x^2-y^2}$) are parallel to each other and practically perpendicular to the exchange pathway. Because of this, the interaction between the magnetic orbitals through the water bridges is poor, and a weak coupling must be expected. The interaction changes from antiferromagnetic to ferromagnetic as the bond angle Cu−O−Cu approaches 90°.

The magnetic susceptibility of compound **4** exhibits a maximum at approximately 200 K and decreases to a minimum value near to 40 K. Below this, there is a rapid increase in magnetic susceptibility as the temperature is lowered further to 2 K. The room temperature magnetic effective moment ($\chi_m T$ = 0.574 cm^{3}K/mol, $\mu_{eff} = 3.03\ \mu_B$) is appreciably lower than that expected for two magnetically noninteracting copper(II) ions even considering the spin-only magnetic moment ($\mu_{eff} = 3.46\ \mu_B$). Upon cooling, $\chi_m T$ continuously decreases, and it practically vanishes at very low temperatures. These features are consistent with strong antiferromagnetic exchange between the two Cu(II) ions. The behavior below 40 K must be a consequence of a small amount of a monomeric Cu(II) compound. According to that, the experimental data can be well described by the Bleaney and Bowers equation[35] combined with an additional term which accounts for uncoupled Cu(II) ions following a simple Curie law, and having the same g factor[36]

$$\chi_m = \frac{(1 - \rho)Ng^2\beta^2}{kT(3 + 3\exp(-J/kT)} + \frac{\rho Ng^2\beta^2}{4kT} \quad (6)$$

where ρ is the percent of noncoupled impurity and other symbols have their usual meanings. An excellent fit to the data (solid lines in Figure 7c) was obtained when $g = 2.13$, $J = -109.7$ cm^{-1}, and $\rho = 0.009$, with an error $R = 8.6 \times 10^{-5}$.

The J value is similar to that shown by a previously reported Cu(II) dimer,[25b] which has bridging ligands of similar nature as well as their relative disposition to those of **4**. However, the J value of the reported compound is slightly lower (−108.3 cm^{-1}) than that for **4**, which may be quite surprising as the intermetallic distance in the latter is slightly longer (2.776 Å) than in the former (2.541 Å). This fact could be justified by the lower asymmetry in the Cu−N bonds of the NCN bridge in **4**, which would reduce the ferromagnetic component of the coupling interaction. In addition, it could be said that the coupling through the NCN bridges contribute in a larger proportion to the J value than the OCO bridges, as the latter ones have the opposite effect.

Photoluminescence Properties. Because of their extended aromaticity and to the presence of polyheterosubstituted hexa- and penta-atomic rings, 1,2,4-triazolo[1,5-*a*]pyrimidine derivatives are good candidates for enhanced emissive properties, tunable, in principle, by coordination to different metals or environments. Recently, a study on the solid-state emission spectra of 7atp and a Zn(II) complex with this ligand was reported by our group.[19] This study revealed that the emission of 7atp is significantly affected by the coordination of the ligand with Zn(II), showing a red-shift of ∼30 nm. On the other hand, there are no previously reported studies on photoluminescent emission for 5HtpO or any of its metal complexes. Luminescence properties have been described though for another oxo-derivative, 5-methyl-7-oxo derivative (commonly known as HmtpO) and some of its platinum(II) complexes.[37]

Both 7atp and 5HtpO ligands show luminescence at room temperature in aqueous solution, however, only 7atp displays characteristic excitation and emission spectra in solid state. For 7atp, using a 316 nm incident radiation, an intense emission band around 420 nm and weaker but sharper ones at 362 and 389 nm are observed. In addition to this, a broad band in the 480−560 nm range also appears. The Zn(II) dinuclear complex **2** has, however, a significantly different emission spectrum (Figure 8) by exciting at its also different absorption maximum, 308 nm. According to previous reports about zinc and cadmium complexes with azolate ligands,[38] the main emission band may

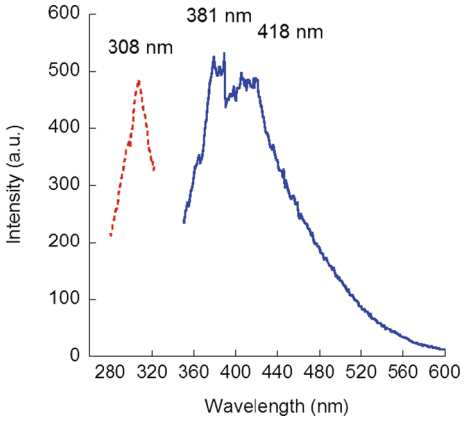

Figure 8. Solid-state excitation and emission spectra of the Zn(II) complex **2**.

be assigned to a ligand-to-ligand electronic transition, which is affected by the coordination of the ligand to the Zn(II) atom.

Final Remarks on the Chemical Analogy with Purines and Biological Implications. The aforementioned parallelism between 7atp and 5HtpO derivatives and adenine and xanthine nucleobases is not only related to their structural similarity (see Scheme 1) but it goes beyond it and is reflected in their coordination behavior. Despite of the different atomic arrangement of triazolopyrimidines, the Lewis basicity seems to be located at the same positions than for their respective biological counterparts, as it is shown by the structures of previously reported coordination complexes with nucleobases.

The characteristic paddle-wheel structure of 7atp-compounds **1** and **2** have been shown previously by a wide range of metal complexes of adenine with several transition metal ions like Co(II), Ni(II) or Ag(I), among others.[23,39−41] However, there are some general differences between 7atp- and adenine-systems: the longer M···M distances for those containing 7atp (differing until ca. 0.5 Å), and the higher number of intermolecular hydrogen bonds in adenine systems, due to purine pyrimidinic ring has an additional nitrogen atom (N1) that is able to interact with neighbor species, and also due to the presence of an acidic proton in the five-membered ring.

Many similarities in the binding preference of the oxo-derivative 5HtpO are also found with its nucleobase analogue, xanthine. As for 5HtpO, previously reported metal complexes with xanthine derivatives show that the preferred coordination mode of this naturally occurring nucleobase depends strongly on its protonation state, being the most frequent mode N9-monodentate followed by μ-N3,N9 and μ-N7,N9 bridges, and being the binding through the oxygen atom more rare.[42]

In general, these findings state a significant grade of analogy in terms of reactivity between 1,2,4-triazolo[1,5-*a*]pyrimidines and biologically relevant molecules as purines. Consequently, potential biological applications not only can be expected for metal complexes containing this type of ligands but some of them have already shown to be promising therapeutic agents, especially against some tropical parasitic diseases like leishmaniasis or Chagas.[5]

CONCLUSIONS

Herein we have described the synthesis and characterization of the first mixed-ligand complexes containing a substituted 1,2,4-triazolo[1,5-*a*]pyrimidine derivative, namely 7atp and 5HtpO, and a malonate or succinate anion. The results show the great diversity of coordination modes that primary and secondary ligands display in this relatively small set of compounds, leading in all cases to dinuclear and polynuclear structures with a complex supramolecular networking built from hydrogen bonds and $\pi-\pi$ interactions. A structural correlation with metal−organic systems containing nucleobase analogues can be established, showing a biomimetic character for triazolopyrimidine-based metal complexes.

The magnetic properties of the paramagnetic complexes are, as may be expected, strongly dependent on the nature of the intermetallic bridging moieties and they range from antiferromagnetic (compounds **1** and **3**) to ferromagnetic interactions (compound **4**). For Cu(II) complexes, this results from changing the dicarboxylate from malonate to succinate while containing both the same triazolopyrimidine ligand. Moreover, it has been shown that the extended aromaticity which is inherent to triazolopyrimidine molecules provides the possibility to yield photoactive compounds, even in solid state and at room temperature as in case of 7atp ligand, whose emissive properties can be modified by changing the metal ion to coordinate. In summary, these preliminary results pave the way for a future work to design, in a somewhat more controllable way, new metal−organic systems based on biomimetic molecules, which may show enhanced physical properties ranging from molecular magnets to luminescence-based sensors or catalytic or gas-storage related applications. In addition, these results become particularly interesting if we consider the already proved bioactivity of triazolopyrimidine derivatives, which may aim future efforts toward a more rational synthesis of, for instance, biodegradable polymers for drug delivery.

ASSOCIATED CONTENT

Supporting Information

Figures S1 (TG and DSC diagrams of compound **4**), S2 (room temperature X-band EPR spectrum of compound **1**), S3 (room temperature Q-band EPR spectrum of compound **3**), and S4 (plot of the reduced magnetization ($M/N\beta$) vs H for **3**); Table S1 (selected bond distances for **1**−**5**), and X-ray crystallographic information and structure factors files for **1**−**5** (CCDC reference numbers: 835133−37).This material is available free of charge via the Internet at http://pubs.acs.org.

AUTHOR INFORMATION

Corresponding Author

*Fax: +34 958248526. Tel: +34 958248525. E-mail: jsalas@ugr.es.

Notes

The authors declare no competing financial interest.

ACKNOWLEDGMENTS

We thank financial support by the Junta de Andalucía (FQM-3705 and FQM-4228). A. B. Caballero thanks the Spanish Ministry of Education for a FPU fellowship.

REFERENCES

(1) (a) Richards, A. D.; Rodger, A. *Chem. Soc. Rev.* **2007**, *36*, 471−483. (b) Chifotides, H. T.; Dunbar, K. R. *Acc. Chem. Res.* **2005**, *38*, 146−156. (c) Navarro, J. A. R.; Lippert, B. *Coord. Chem. Rev.* **2001**, *222*, 219−250.

(2) Hannon, M. J. *Chem. Soc. Rev.* **2007**, *36*, 280−295.

(3) Legraverend, M.; Grierson, D. S. *Bioorg. Med. Chem.* **2006**, *14*, 3987−4006.

(4) (a) Rojas-González, P. X.; Castiñeiras, A.; González-Pérez, J. M.; Choquesillo-Lazarte, D.; Niclós-Gutiérrez, J. *Inorg. Chem.* **2002**, *41*, 6190−6192. (b) Zamora, F.; Kunsman, M.; Sabat, M.; Lippert, B. *Inorg. Chem.* **1997**, *36*, 1583−1594.
(5) (a) Luque, F.; Fernández-Ramos, C.; Entrala, E.; Rosales, M. J.; Marín, C.; Salas, J. M.; Navarro, J. A. R.; Sánchez-Moreno, M. *Toxicol In Vitro* **2000**, *14*, 487−495. (b) Luque, F.; Fernández-Ramos, C.; Entrala, E.; Rosales, M. J.; Navarro, J. A. R.; Romero, M. A.; Salas, J. M.; Sánchez-Moreno, M. *Comp. Biochem. Physiol., C: Comp. Pharmacol.* **2000**, *126*, 39−44. (c) Magán, R.; Marín, C.; Rosales, M. J.; Barrera, M. A.; Salas, J. M.; Sánchez-Moreno, M. *Pharmacology* **2004**, *70*, 83−90. (d) Magán, R.; Marín, C.; Rosales, M. J.; Salas, J. M.; Sánchez-Moreno, M. *Pharmacology* **2005**, *73*, 41−48. (e) Boutaleb-Charki, S.; Marín, C.; Maldonado, C. R.; Rosales, M. J.; Urbano, J.; Gutiérrez-Sánchez, R.; Quirós, M.; Salas, J. M.; Sánchez-Moreno, M. *Drug Metab. Lett.* **2009**, *3*, 35−44. (f) Maldonado, C. R.; Marin, C.; Olmo, F.; Huertas, O.; Quirós, M.; Sánchez-Moreno, M.; Rosales, M. J.; Salas, J. M. *J. Med. Chem.* **2010**, *53*, 6964−6972. (g) Salas, J. M.; Quirós, M.; Abul-Haj, M.; Magán, R.; Marín, C.; Sánchez-Moreno, M.; Faure, R. *Met.-Based Drugs* **2001**, *8*, 119−124. (h) Ramírez-Macías, I.; Marín, C.; Salas, J. M.; Caballero, A.; Rosales, M. J.; Villegas, N.; Rodríguez-Diéguez, A.; Barea, E.; Sánchez-Moreno, M. *J. Antimicrob. Chemother.* **2011**, *66*, 813−819. (i) Caballero, A. B.; Marín, C.; Rodríguez-Diéguez, A.; Ramírez-Macías, I.; Barea, E.; Sánchez-Moreno, M.; Salas, J. M. *J. Inorg. Biochem.* **2011**, *105*, 770−776. (j) Akdi, K.; Vilaplana, R. A.; Kamah, S.; Navarro, J. A. R.; Salas, J. M.; González-Vílchez, F. *J. Inorg. Biochem.* **2002**, *90*, 51−60. (k) Lakowska, I.; Szlyk, E.; Sitkowski, J.; Kozerski, L.; Wietrzyk, J.; Pelczynska, M.; Nasulewicz, A.; Opolski, A. *J. Inorg. Biochem.* **2004**, *98*, 167−172. (l) Navarro, J. A. R.; Salas, J. M.; Romero, M. A.; Vilaplana, R.; González-Vílchez, F.; Faure, R. *J. Med. Chem.* **1998**, *41*, 332−338. (m) Lakomska, I. *Inorg. Chim. Acta* **2009**, *362*, 669. (n) Ruiz, J.; Villa, M. D.; Cutillas, N.; López, G.; de Haro, C.; Bautista, D.; Moreno, V.; Valencia, L. *Inorg. Chem.* **2008**, *47*, 4490−4505. (o) Lakomska, I.; Kooijman, H.; Spek, A. L.; Shen, W.; Reedijk, J. *J. Chem. Soc., Dalton Trans.* **2009**, 10736−10741. (p) Velders, A. H.; Bergamo, A.; Alessio, E.; Zangrando, E.; Haasnoot, J. G.; Casarsa, C.; Cocchietto, M.; Zorzet, S.; Sava, G. *J. Med. Chem.* **2004**, *47*, 1110−1121. (q) Zhang, N.; Ayral-Kaloustian, S.; Nguyen, T.; Afragola, J.; Hernández, R.; Lucas, J.; Gibbons, J.; Beyer, C. *J. Med. Chem.* **2007**, *50*, 319−327.
(6) Salas, J. M.; Romero, M. A.; Sánchez, M. P.; Quirós, M. *Coord. Chem. Rev.* **1999**, *193*−*195*, 1119−1142.
(7) Caballero, A. B.; Rodríguez-Diéguez, A.; Lezama, L.; Barea, E.; Salas, J. M. *Dalton Trans.* **2011**, *40*, 5180−5187.
(8) Caballero, A. B.; Marín, C.; Ramírez-Macías, I.; Rodríguez-Diéguez, A.; Quirós, M.; Salas, J. M.; Sánchez-Moreno, M. *Polyhedron* **2012**, *33*, 137−144.
(9) (a) Caballero, A. B.; Rodríguez-Diéguez, A.; Vieth, J. K.; Salas, J. M.; Janiak, C. *Inorg. Chim. Acta* **2011**, *376*, 674−678. (b) Caballero, A. B.; Rodríguez-Diéguez, A.; Barea, E.; Quirós, M.; Salas, J. M. *CrystEngComm* **2010**, *12*, 3038−3045. (c) Abul Haj, M.; Quirós, M.; Salas, J. M.; Faure, R. *Inorg. Chem. Commun.* **2001**, *4*, 254−256. (d) Abul Haj, M.; Quirós, M.; Salas, J. M. *J. Chem. Soc., Dalton Trans.* **2002**, 4740−4745. (e) Navarro, J. A. R.; Romero., M. A.; Salas, J. M. *J. Chem. Soc., Dalton Trans.* **1997**, 1001−1005. (f) Lekkas, N.; Hadjiliadis, N.; Garoufis, A.; Kobe, J.; Bernhardt, P. V.; Tiekink, E. R. T. *Inorg. Chim. Acta* **2006**, *359*, 4297−4303. (g) Abul Haj, M.; Quirós, M.; Salas, J. M. *Polyhedron* **2004**, *23*, 2373−2379.
(10) Caballero, A. B.; Maclaren, J. K.; Rodríguez-Diéguez, A.; Vidal, I.; Dobado, J. A.; Salas, J. M.; Janiak, C. *Dalton Trans.* **2011**, *40*, 11845−11855.
(11) Caballero, A. B.; Castillo, O.; Lezama, L.; Rodríguez-Diéguez, A.; Salas, J. M. *Inorg. Chem. Commun.* **2012**, *19*, 36−38.
(12) Moulton, B.; Zaworotko, M. J. *Chem. Rev.* **2001**, *101*, 1629−1658.
(13) (a) Rodríguez-Martín, Y.; Hernández-Molina, M.; Delgado, F. S.; Pasán, J.; Ruiz-Pérez, C.; Sanchiz, J.; Lloret, F.; Julve, M. *CrystEngComm* **2002**, 522−535. (b) Rodríguez-Martín, Y.; Hernández-Molina, M.; Delgado, F. S.; Pasán, J.; Ruiz-Pérez, C.; Sanchiz, J.; Lloret, F.; Julve, M. *CrystEngComm* **2002**, 440−446. (c) Ruiz-Pérez, C.; Rodríguez-Martín, Y.; Hernández-Molina, M.; Delgado, F. S.; Pasán, J.; Sanchiz, J.; Lloret, F.; Julve, M. *Polyhedron* **2003**, *22*, 2111−2123. (d) Mao, H.; Zhang, C.; Li, G.; Zhang, H.; Hou, H.; Li, L.; Wu, Q.; Zhub, Y.; Wanga, E. *Dalton Trans.* **2004**, 3918−3925. (e) Demir, S.; Kaya, G. *Z. Anorg. Allg. Chem.* **2011**, *637*, 456−461. (f) Montney, M. R.; Krishnan, S. M.; Patel, N. M.; Supkowski, R. M.; LaDuca, R. L. *Cryst. Growth Des.* **2007**, *7* (6), 1145−1153. (g) Du, M.; Jiang, X.-J.; Zhao, X.-J.; Cai, H.; Ribas, J. *Eur. J. Inorg. Chem.* **2006**, 1245−1254. (h) Zhou, Z.-H.; Yang, J.-M.; Wan, H.-L. *Cryst. Growth Des.* **2005**, *5* (5), 1825−1830 and references therein..
(14) (a) Rodríguez-Martín, Y.; Sanchiz, J.; Ruiz-Pérez, C.; Lloret, F.; Julve, M. *CrystEngComm* **2002**, 631−637. (b) Rodríguez-Martín, Y.; Sanchiz, J.; Ruiz-Pérez, C.; Lloret, F.; Julve, M. *Inorg. Chim. Acta* **2001**, *326*, 20−26. (c) Rodríguez-Martín, Y.; Hernández-Molina, M.; Sanchiz, J.; Ruiz-Pérez, C.; Lloret, F.; Julve, M. *Dalton Trans.* **2003**, 2359−2365. (d) Konar, S.; Mukherjee, P. S.; Drew, M. G. B.; Ribas, J.; Chaudhuri, N. R. *Inorg. Chem.* **2003**, *42*, 2545−2552. (e) Delgado, F. S.; Sanchiz, J.; Ruiz-Pérez, C.; Lloret, F.; Julve, M. *Inorg. Chem.* **2003**, *42*, 5938−5948. (f) Liu, T. F.; Sun, H. L.; Gao, S.; Zhang, S. W.; Lau, T. C. *Inorg. Chem.* **2003**, *42*, 4792−4794. (g) Delgado, F. S.; Sanchiz, J.; Ruiz-Pérez, C.; Lloret, F.; Julve, M. *CrystEngComm* **2003**, *5*, 280−286. (h) Demir, S.; Yilmaz, V. T.; Sariboga, B.; Buyukgungor, O.; Mrozinski, J. *J. Inorg. Organomet. Polym.* **2010**, *20*, 220−228 and references therein..
(15) Abul Haj, M.; Salas, J. M.; Quirós, M.; Molina, J.; Faure, R. *J. Mol. Struct.* **2000**, *519*, 165−172.
(16) *Apex2, Data Collection Program for the CCD Area-Detector System*; *SAINT, Data Reduction and Frame Integration Program for the CCD Area-Detector System*; Bruker Analytical X-ray Systems: Madison, WI, U.S.A., 1997−2006.
(17) Sheldrick, G. *SADABS: Area-detector absorption correction*; University of Göttingen: Göttingen, Germany, 1996.
(18) Altomare, A; Burla, M. C.; Camilla, M.; Cascarano, G. L.; Giacovazzo, C.; Guagliardi, A.; Moliterni, A. G. G.; Polidori, G.; Spagna, R. *J. Appl. Crystallogr.* **1999**, *32*, 115−119.
(19) Sheldrick, G. M. *Acta Crystallogr. A* **2008**, *64*, 112−122.
(20) Caballero, A. B.; Rodriguez-Dieguez, A.; Quirós, M.; Lezama, L.; Salas, J. M. *Inorg. Chim. Acta* **2011**, *378* (1), 194−201.
(21) Abul Haj, M.; Quirós, M.; Salas, J. M.; Faure, R. *J. Chem. Soc., Dalton Trans.* **2001**, 1798−1801.
(22) Abul Haj, M.; Quirós, M.; Salas, J. M.; Dobado, J. A.; Molina, J.; Basallote, M. G.; Máñez, M. A. *Eur. J. Inorg. Chem.* **2002**, 811−818.
(23) Caballero, A. B.; Rodríguez-Diéguez, A.; Vidal, I.; Dobado, J. A.; Castillo, O.; Lezama, L.; Salas, J. M. *Dalton Trans.* **2012**, *41*, 1755−1764.
(24) $\tau_5 = (\beta - \alpha)/60$, where β and α are, respectively, the major angles of the metal ion coordination sphere, being $\tau_5 = 0$ for a square pyramidal geometry, and $\tau_5 = 1$ for a trigonal bipyramidal geometry.
(25) (a) Goodgame, D. M. L.; Nishida, Y.; Winpenny, R. E. P. *Bull. Chem. Soc. Jpn.* **1986**, *59*, 344−346. (b) Gutiérrez, L.; Alzuet, G.; Borrás, J; Castiñeiras, A.; Rodríguez-Fortea, A.; Ruiz, E. *Inorg. Chem.* **2001**, *40*, 3089−3096. (c) Caballero, A. B.; Rodríguez-Diéguez, A.; Vidal, I.; Dobado, J. A.; Castillo, O.; Lezama, L.; Salas, J. M. *Dalton Trans.* **2011**, *41*, 1755−1764.
(26) Ozarowski, A. *Inorg. Chem.* **2008**, *47*, 9760−9762.
(27) Bencini, A; Gatteschi, D. *EPR of Exchange Coupled Systems*; Springer Verlag: Berlin, 1990.
(28) Abragam, A; Bleaney, B. *Electron Paramagnetic Resonance of Transition Ions*; Dover Publications, Inc.: New York, 1986.
(29) van Vleck, J. H. *The Theory of Electric and Magnetic Susceptibilities*; Oxford University Press: Oxford, U.K., 1932.
(30) Sonnenfroh, D.; Kreilick, R. W. *Inorg. Chem.* **1980**, *19*, 1259−1262.
(31) (a) Delgado, F. S.; Hernández-Molina, M.; Sanchiz, J.; Ruiz-Pérez, C.; Rodríguez-Martín, Y.; López, T.; Lloret, F.; Julve, M. *CrystEngComm* **2004**, *6*, 106−111. (b) Cañadillas-Delgado, L.; Fabelo,

O.; Pasán, J.; Delgado, F. S.; Lloret, F.; Julve, M.; Ruiz-Pérez, C. *Inorg. Chem.* **2007**, *46*, 7458−7465.
(32) (a) Nishida, Y.; Kida, S. *J. Chem. Soc., Dalton Trans.* **1986**, 2633−2640. (b) McKee, V.; Zvagulis, M.; Reed, C. A. *Inorg. Chem.* **1985**, *24*, 2914−2919.
(33) Pérez-Yáñez, S.; Castillo, O.; Cepeda, J.; García-Terán, J. P.; Luque, A.; Román, P. *Eur. J. Inorg. Chem.* **2009**, 3889−3899.
(34) Franceschi, F.; Guillemot, G.; Solari, E.; Floriani, C.; Re, N.; Birkedal, H.; Pattison, P. *Chem.—Eur. J.* **2001**, *7* (7), 1468−1478.
(35) Bleaney, B.; Bowers, K. D. *Proc. R. Soc. London, Ser. A* **1952**, *214*, 451−465.
(36) Kahn, O. *Molecular Magnetism*; VCH: New York, 1993.
(37) Belisle, H.; Reber, C. *Can. J. Anal. Sci. Spect.* **2003**, *48*, 24−29.
(38) (a) Seco, J. M.; de Araujo Farias, M.; Bachs, N. M.; Caballero, A. B.; Salinas-Castillo, A.; Rodriguez-Dieguez, A. *Inorg. Chim. Acta* **2010**, *363* (13), 3194−3199. (b) Wang, X.-S.; Tang, Y.-Z.; Huang, X.-F.; Qu, Z.-R.; Che, C.-M.; Chang, P.-W.-H.; Xiong, R.-G. *Inorg. Chem.* **2005**, *44*, 5278−5285.
(39) Pérez-Yáñez, S.; Castillo, O.; Cepeda, J.; García-Terán, J. P.; Luque, A.; Román, P. *Eur. J. Inorg. Chem.* **2009**, 3889−3899.
(40) (a) Sletten, E. *Acta Crystallogr., Sect. B* **1969**, *25*, 1480−1491. (b) Sanz Miguel, P. J.; Lippert, B. *Dalton Trans.* **2005**, 1679−1696. (c) Beatty, A. M. *Coord. Chem. Rev.* **2003**, *246*, 131−143. (d) Burda, J. V.; Gu, J. *J. Inorg. Biochem.* **2008**, *102*, 53−62. (e) Kickelbick, G. *Hybrid Materials: Synthesis Characterisation, and Applications*; Wiley-VCH: Weinheim, Germany, 2007. (f) Horcajada, P.; Serre, C.; Vallet-Regi, M.; Sebban, M.; Taulelle, F.; Férey, G. *Angew. Chem., Int. Ed.* **2006**, *45*, 5974−5978. (g) Hupp, J. T.; Poeppelmeier, K. R. *Science* **2005**, *309*, 2008−2009. (h) Terzis, A.; Beauchamp, A. L.; Rivest, R. *Inorg. Chem.* **1973**, *12*, 1166−1170. (i) de Meester, P.; Skapski, A. C. *J. Chem. Soc. A* **1971**, *13*, 2167−2169. (j) González-Pérez, J. M.; Alarcón-Payer, C.; Castiñeiras, A.; Pivetta, T.; Lezama, L.; Choquesillo-Lazarte, D.; Crisponi, G.; Niclós-Gutiérrez, J. *Inorg. Chem.* **2006**, *45*, 877−882. (k) García-Terán, J. P.; Castillo, O.; Luque, A.; García-Couceiro, U.; Román, P.; Lezama, L. *Inorg. Chem.* **2004**, *43*, 4549−4551.
(41) (a) Fondo, M.; Ocampo, N.; García-Deibe, A. M.; Corbella, M.; El Fallah, M. S.; Cano, J.; Sanmartin, J.; Bermejo, M. R. *Dalton Trans.* **2006**, 4905−4913. (b) Pajunen, A.; Nasakkala, E. *Finn. Chem. Lett.* **1977**, *4*, 100−103. (c) Fondo, M.; García-Deibe, A. M.; Ocampo, N.; Sanmartin, J.; Bermejo, M. R.; Llamas-Saiz, A. L. *Dalton Trans.* **2006**, 4260−4270.
(42) (a) Yuan, H. Q.; Aoki, K.; Fujisawa, I. *Inorg. Chim. Acta* **2009**, *362*, 975−984. (b) Dubler, E.; Hanggi, G.; Schmalle, H. *Inorg. Chem.* **1992**, *31*, 3728−3736. (c) Colacio, E.; Cuesta, R.; Gutiérrez-Zorrilla, J. M.; Luque, A.; Román, P.; Giraldi, T.; Taylor, M. R. *Inorg. Chem.* **1996**, *35*, 4232−4238. Mikulski, C. M.; Kurlan, M. K.; Bayne, M.; Gaul, M. *Inorg. Chim. Acta* **1986**, *123*, 27−33. (e) Salas-Peregrín, J. M.; Colacio-Rodríguez, E.; Romero-Molina, M. A.; Sánchez-Sánchez, M. P. *Thermochim. Acta* **1983**, *69*, 313−321.